

UC Office of the President

Recent Work

Title

Sequence-Specific Electrical Purification of Nucleic Acids with Nanoporous Gold Electrodes

Permalink

<https://escholarship.org/uc/item/3cs3d2h3>

Authors

Daggumati, Pallavi
Appelt, Sandra
Matharu, Zimple
et al.

Publication Date

2016-05-31

DOI

10.1021/jacs.6b03563

Peer reviewed

Sequence-Specific Electrical Purification of Nucleic Acids with Nanoporous Gold Electrodes

Pallavi Daggumati, Sandra Appelt, Zimple Matharu, Maria Marco, and Erkin Seker

J. Am. Chem. Soc., **Just Accepted Manuscript** • DOI: 10.1021/jacs.6b03563 • Publication Date (Web): 31 May 2016

Downloaded from <http://pubs.acs.org> on May 31, 2016

Just Accepted

“Just Accepted” manuscripts have been peer-reviewed and accepted for publication. They are posted online prior to technical editing, formatting for publication and author proofing. The American Chemical Society provides “Just Accepted” as a free service to the research community to expedite the dissemination of scientific material as soon as possible after acceptance. “Just Accepted” manuscripts appear in full in PDF format accompanied by an HTML abstract. “Just Accepted” manuscripts have been fully peer reviewed, but should not be considered the official version of record. They are accessible to all readers and citable by the Digital Object Identifier (DOI®). “Just Accepted” is an optional service offered to authors. Therefore, the “Just Accepted” Web site may not include all articles that will be published in the journal. After a manuscript is technically edited and formatted, it will be removed from the “Just Accepted” Web site and published as an ASAP article. Note that technical editing may introduce minor changes to the manuscript text and/or graphics which could affect content, and all legal disclaimers and ethical guidelines that apply to the journal pertain. ACS cannot be held responsible for errors or consequences arising from the use of information contained in these “Just Accepted” manuscripts.

Sequence-Specific Electrical Purification of Nucleic Acids with Nanoporous Gold Electrodes

Pallavi Daggumati¹, Sandra Appelt², Zimple Matharu¹, Maria Marco², and Ekin Seker^{1*}

¹Department of Electrical and Computer Engineering, University of California - Davis, Davis, California 95616, United States

²Department of Food Science & Technology, University of California - Davis, Davis, California 95616, United States

ABSTRACT

Nucleic acid-based biosensors have enabled rapid and sensitive detection of pathogenic targets; however, these devices often require purified nucleic acids for analysis since the constituents of complex biological fluids adversely affect sensor performance. This purification step is typically performed outside the device, thereby increasing sample-to-answer time and introducing contaminants. We report a novel approach using a multifunctional matrix, nanoporous gold (np-Au), which enables both detection of specific target sequences in a complex biological sample and their subsequent purification. The np-Au electrodes modified with 26-mer DNA probes (via thiol-gold chemistry) enabled sensitive detection and capture of complementary DNA targets in the presence of complex media (fetal bovine serum) and other interfering DNA fragments in the range 50 to 1500 base pairs. Upon capture, the non-complementary DNA fragments and serum constituents of varying sizes were washed away. Finally, the surface-bound DNA-DNA hybrids were released by electrochemically cleaving the thiol-gold linkage and the hybrids were iontophoretically eluted from the nanoporous matrix. The optical and electrophoretic characterization of the analytes before and after the detection-purification process revealed that low target DNA concentrations (80 pg/ μ L) can be successfully detected in complex biological fluids and subsequently released to yield pure hybrids free of polydisperse digested DNA fragments and serum biomolecules. Taken together, this multifunctional platform is expected to enable seamless integration of detection and purification of nucleic acid biomarkers of pathogens and diseases in miniaturized diagnostic devices.

INTRODUCTION

1
2
3
4
5 With the advent of nanostructured materials, nucleic acid-based biosensors for pathogen detection
6 have exhibited enormous progress during the last decade¹⁻³. Miniaturization of the sensor platform
7 coupled with phenomena unique to nanoscale⁴ enabled faster sensor response, lower limits of
8 detection, and reduced reagent volumes compared to traditional benchtop methods^{5,6}. However, in
9 order to benefit from these features, most sensing platforms still require sample preparation,
10 particularly purification of nucleic acids from complex biological samples⁷. Traditional benchtop
11 (off-chip) processes for DNA extraction often utilize phase separation, where proteins in the
12 complex sample are denatured or aggregated, DNA is precipitated with alcohols or physisorbed to
13 a solid phase support, and DNA is finally recovered through centrifugation or elution^{8,9}. In order
14 to achieve a complete sample-in-answer-out system, it is imperative to integrate sample
15 preparation and detection modalities. While DNA capture via solid phase supports, such as ones
16 created by packing microfluidic channels with silica beads or embedding the beads in sol-gel
17 matrices^{10,11}, is more conducive to integration into miniaturized nucleic acid interrogation
18 platforms, these devices still suffer from mechanical instability, including matrix shrinkage
19 compromising DNA extraction efficiency^{12,13}. In order to mitigate the mechanical issues and low
20 reproducibility while maintaining a high surface area-to-volume ratio for efficient DNA capture,
21 top-down photolithographic approaches were used to incorporate pillars in microfluidic channels¹⁴
22 with various materials, including silica¹⁵, poly(methyl methacrylate)¹⁶, and polycarbonate¹⁷.
23 However, the complex microfabrication processes to create these high aspect ratio structures have
24 limited their feasibility. Other non-traditional techniques, such as use of paramagnetic particles¹⁸
25 and hydrophobic magnetic ionic liquids¹⁹ for magnetic capture and release of DNA presented
26 procedural challenges that required complex system design to incorporate magnets required for
27 DNA capture. In summary, a major obstacle to realizing sample-in-answer-out platforms remains
28 to be the lack of seamless integration of sample preparation and analysis modalities.
29
30
31
32
33
34
35
36
37
38
39
40
41
42
43
44
45
46
47
48

49 In order to address this significant need, we present a novel approach for integrated electrical
50 detection and purification of DNA in complex biological samples using nanoporous gold (np-Au)
51 as a multifunctional electrode coating. Owing to its catalytic properties, tunable morphology,
52 microfabrication compatibility and excellent thiol-gold chemistry, np-Au is an emerging material
53 for biosensing applications²⁰⁻²². We recently demonstrated that np-Au electrochemical sensors
54
55
56
57
58
59
60

1
2
3 exhibit excellent biofouling-resilience in the presence of complex media such as serum while
4 preserving the sensitive DNA detection capabilities^{23,24}. In addition, as the np-Au thin film
5 electrodes can be easily produced using conventional microfabrication techniques, they are highly
6 amenable to seamless integration with microfluidics and other microsystem components to build
7 complete sample-in-answer-out platforms²⁵. Leveraging these features, the two-part purification
8 approach demonstrated here enables both the electrochemical detection of DNA targets of interest
9 in the presence of complex media (fetal bovine serum, FBS) as well as subsequent electrokinetic
10 release of the DNA-DNA hybrids free of contaminants (e.g., serum macromolecules and
11 mismatched DNA fragments) for additional downstream analysis.
12
13
14
15
16
17
18
19

20 RESULTS AND DISCUSSION

21
22 **Concept of the purification device.** The np-Au electrodes were fabricated using a hybrid
23 approach that merges conventional microfabrication processes and self-assembled nanostructured
24 material synthesis, as described previously²⁴. Morphological characterization via scanning
25 electron microscopy (SEM) and subsequent image analysis revealed a median pore radius of 15
26 nm. (Figure 1A). The residual silver in np-Au samples after dealloying was estimated to be ~8%
27 (atomic %) via EDS. The concept of capture and electrochemical detection of target DNA
28 molecules, followed by electrokinetic release of the hybrids, is illustrated in Figure 1. In order to
29 characterize the platform, we used a unique 26-mer housekeeping region of the DNA sequence of
30 tobacco mosaic virus (TMV) as a target sequence. The np-Au electrodes were functionalized with
31 thiolated ssDNA (26-mer) specific to the target of interest (i.e., TMV). The details of the DNA
32 sequence, sensor preparation, and electrochemical setup are described in the Experimental
33 Methods section. Methylene blue (MB) redox marker was used for quantifying the extent of target
34 hybridization. The electrode was challenged with a complex mixture (FBS solution (10%) spiked
35 with specific 26-mer target DNA and/or DNA digests containing several DNA fragments with
36 strand length of 50 bp to 1500 bp). Previous studies by us and others have suggested that
37 macromolecules in FBS, such as globular proteins (e.g., albumin), are too large to go through the
38 np-Au pores while the short, fiber-like, nucleic acids can penetrate the porous network, thereby
39 rendering np-Au electrodes biofouling-resilient^{23,26}. Owing to this selective transport, it is possible
40 to electrochemically characterize probe-target hybridization of specific target sequences. The large
41 biomolecules (present in FBS), non-hybridized DNA fragments were then washed away using
42 phosphate buffer. The captured nucleic acids were released by electrochemically-cleaving the
43
44
45
46
47
48
49
50
51
52
53
54
55
56
57
58
59
60

thiol-gold bond²⁷. Desorption of the hybrids was confirmed by an optical assay utilizing PicoGreen, which is a probe that forms a highly fluorescent complex upon specific binding with double-stranded DNA (dsDNA)²⁸. We further evaluated the efficacy of the purification process by performing capillary electrophoresis on the samples before and after purification.

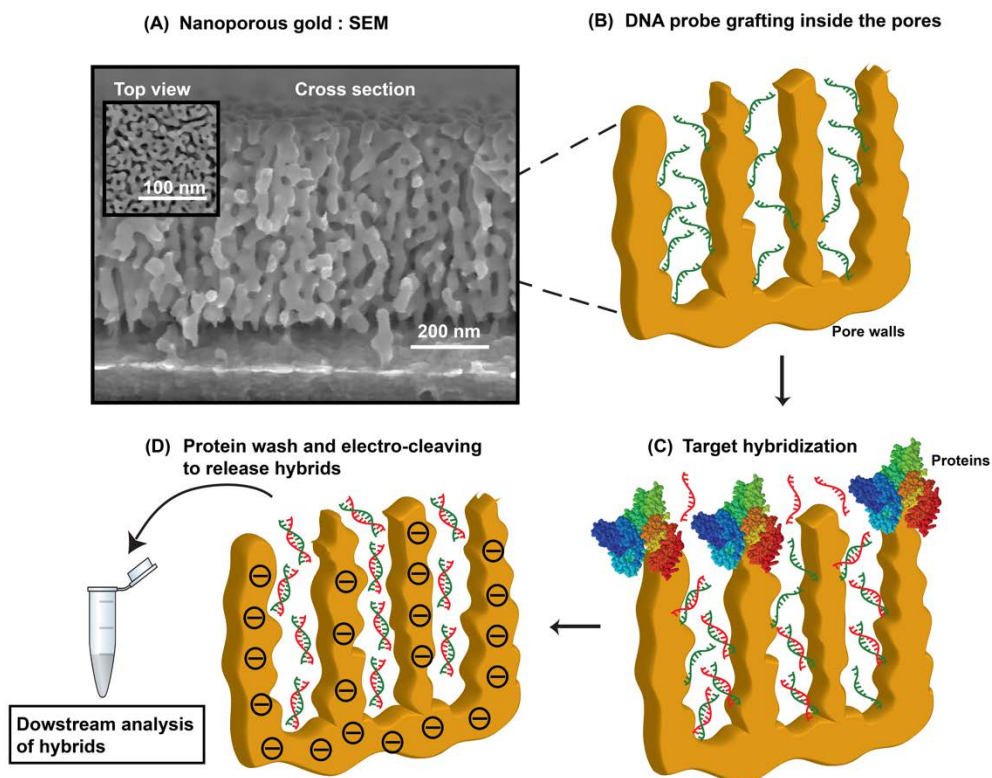


Figure 1. (A) Scanning electron micrographs of np-Au electrode. (B) Thiol-immobilized ssDNA capture probes inside the porous structure. (C) Selective transport of target molecules into the pores while macromolecules (e.g., proteins and other components of FBS) are blocked at the pore entrances. (D) Protein wash and electrochemical cleaving of DNA-DNA hybrids in a low ionic strength buffer. Downstream analysis of eluted hybrids via fluorescence (hybrid concentration), absorbance (DNA-to-protein concentration ratio), and capillary electrophoresis (hybrid size and purity).

Target capture and electrokinetic release of hybrids. In this section, we discuss the results of the electrical purification process and various parameters optimized to improve the DNA extraction. We used methylene blue (MB) redox marker for electrochemical DNA detection and quantification due to its reaction-limited nature (hence ability to permeate the porous structure

before being fully depleted at the top surface) and the ability to discriminate dsDNA from single-stranded DNA (ssDNA)²⁹. The np-Au electrodes were immobilized with ssDNA probes and their response to MB was interrogated via square wave voltammetry (SWV) to reduce the influence of significant capacitive current due to the large effective surface area of the np-Au electrodes. All stated electrochemical potentials are with reference to Ag/AgCl electrode. The total number of grafted probes was estimated to be 4.3×10^{12} molecules, which translates into a grafting density that is 10 times that of its planar gold counterpart²⁴. This 10-fold increase in the grafting density is in agreement with the surface area enhancement, indicating that most of the porous surface of the electrode is covered with recognition molecules and MB molecules can access the deeper surfaces of the porous electrode²⁴. We then challenged the sensor with the DNA target spiked into FBS solution to simulate the complex environment. We used a loading concentration of 300 nM (2.4 ng/ μ L), as this corresponds to the concentration that led to sensor saturation in our previous study²⁴. Upon target hybridization, the SWV peak current dropped, indicating successful target hybridization (Figure 2A). The number of resultant hybrids was estimated by multiplying the percent signal suppression by the total number of ssDNA with the assumption that the majority of the signal drop is due to the hybridized probes²⁹. This was followed by washing off the FBS constituents and electrochemical cleaving to release the thiol-bound hybrids via cyclic voltammetry (CV).

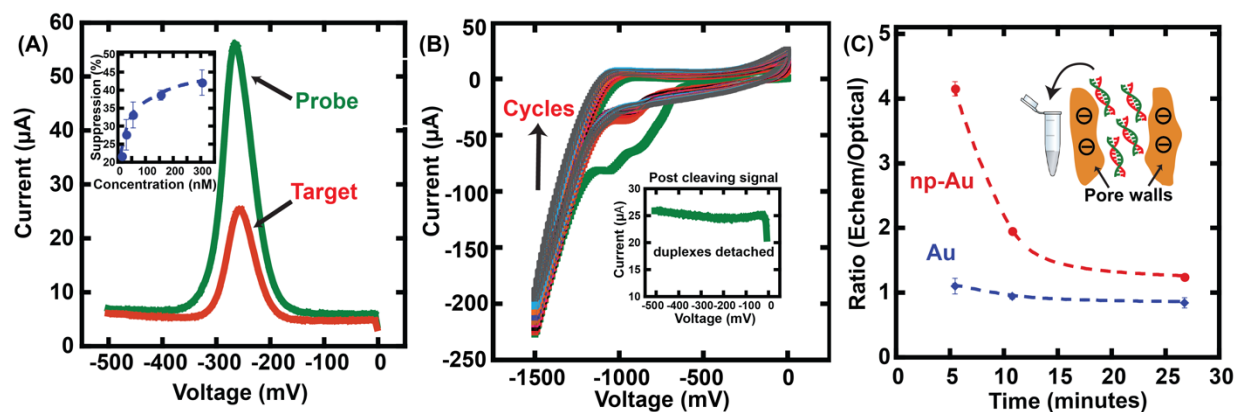


Figure 2. (A) Target DNA detection: Square wave voltammograms (SWV) of probe DNA and target DNA after hybridization. The difference in peak current (at ~ -265 mV) is used to quantify the extent of hybridization. Inset: Target hybridization calibration curve where signal suppression is $(I_{\text{probe}} - I_{\text{target}} / I_{\text{probe}}) \times 100$ (B) Hybrid cleaving: Cyclic voltammograms (CV) in 25 mM phosphate buffer (hybrid elution buffer)

1
2
3 at 10 mV/s. Inset: SWV signal after hybrid cleaving: Absence of a reduction peak indicates that DNA
4 hybrids are not anchored onto the surface. (C) Ratio (Electrochemical hybrid density estimate to optical
5 hybrid density estimate) vs. the duration at reductive negative potentials for each scan rate. Inset: Ratio
6 (Electrochemical hybrid density estimate to optical hybrid density estimate) vs. CV scan rate on np-Au and
7 planar Au electrodes.
8
9
10

11
12
13 Onset of the thiol bond reduction typically occurs around -0.65 V^{27} , but it has been shown that
14 desorption of surface-bound thiolated molecules happens with much higher efficiency at -1.3 V^{30} .
15 To that end, in order to ensure complete removal of the surface-bound hybrids and to minimize
16 their re-adsorption, we used CV in the range of 0 to -1.5 V at scan rates between 10 mV/s to 50
17 mV/s (Figure 2B). Even though the release of hybrids from planar surfaces (e.g., planar gold²⁷ and
18 indium tin oxide³¹) is almost instantaneous, for the case of np-Au, transport of the desorbed hybrids
19 through the porous structure is hindered due to surface-molecule interactions and tortuosity of the
20 np-Au electrode³². We therefore employed multiple CV cycles at negative potentials to enhance
21 iontophoretic elution of the negatively-charged hybrids into a 25 mM phosphate buffer³³. There
22 was no SWV peak present after the cleaving process (Figure 2B inset), indicating the successful
23 desorption of the duplexes from the np-Au surfaces. In order to confirm that the loss of
24 electrochemical signal was due to the absence of duplexes rather than the residual redox molecules,
25 the sensor was further interrogated via SWV following additional MB loading. Observation of a
26 broad peak (Figure S1) confirmed that this signal is mostly due to surface-MB reactions.
27
28
29
30
31
32
33
34
35
36
37
38

39 **Quantification of duplex elution efficiency.** Desorption and elution of hybrids was further
40 confirmed by adding PicoGreen stain (Thermo Fisher Scientific) to the eluted hybrids. The
41 concentration of the eluted hybrids was then determined via fluorospectrometry (Nanodrop 3300)
42 (dye calibration details in the SI, Figure S2). The ratio of the electrochemically-determined hybrid
43 concentration (extracted from the SWV signal suppression) to the optically-determined hybrid
44 concentration with respect to varying cyclic voltammetry scan rates was estimated. The ratio
45 serves as an indicator of *duplex elution efficiency*. A ratio closer to 1 indicates that the
46 electrochemical hybrid density estimate matches well with the optical estimate, suggesting that
47 majority of the duplexes are desorbed and released into the elution buffer. In case of planar gold,
48 this ratio is independent of the scan rate since the duplexes are not hindered by the presence of a
49 porous network, that is, once the thiol link is cleaved, the duplexes are released straight into the
50
51
52
53
54
55
56
57
58
59
60

1
2
3 elution buffer. However, in the case of np-Au, the ratio increases as scan rate increases, because
4 at high scan rates, desorption is not efficient as the duplexes do not have enough time to exit the
5 entire porous structure. At 10 mV/s, the duration spent (26 minutes) at negative potentials above
6 the critical thiol reduction potential is long enough for the cleaved duplexes to exit the porous
7 structure (Figure 2C). Consequently, for this scan rate the ratio approaches ~1, indicating mostly
8 complete elution of the desorbed hybrids. In contrast, when the duplexes were detached by using
9 dithiothreitol (DTT), a common thiol-bond cleaving agent, and no negative potential was applied,
10 the elution of the detached duplexes was significantly hindered (Figure S3). Further investigation
11 of the effect of the number of cycles and cleaving steps, as illustrated in the SI, revealed that for
12 CV at 10 mV/s and 20 cycles, the optimized ratio was 1.23. These conditions were used for the
13 subsequent studies.

23
24 **Target capture efficiency.** Another performance metric for the sensing-purification platform is
25 *target capture efficiency*, which is the amount of eluted hybrids recovered after purification as a
26 percentage of the initial target loading concentration (i.e., target DNA of interest spiked into FBS).
27 This is an important metric, as the ability to capture and purify low levels of a DNA target is
28 essential for detection and further characterization of biomarkers. For the initial sensing step, np-
29 Au sensor exhibited a dynamic range of detection between 10 nM to 150 nM and signal saturation
30 at 150 nM with a signal suppression of ~40% (Figure 3). For the purification step, the optical
31 quantification of the eluted duplexes revealed that the target capture efficiency decreased from
32 ~75% at lower target loading concentrations to ~15% at high concentrations (Figure 3). The
33 substantial decrease in the capture efficiency for high loading concentrations is attributed to the
34 saturation of the capture probes on the np-Au network. In other words, there remains an
35 appreciable amount of unhybridized target DNA that is removed during the wash step. Whereas at
36 low concentrations, a significant portion of the loaded target DNA hybridizes with the probes and
37 is subsequently released from the np-Au electrode. In order to assess the efficiency in removing
38 proteins during the purification step, we acquired the absorbance values at 260 nm (characteristic
39 to DNA) and 280 nm (characteristic to proteins). The resulting absorbance ratio, A_{260}/A_{280} (with
40 1.8 generally indicating high purity) is indicative of the relative amount of protein contaminants
41 in DNA samples³⁴. The A_{260}/A_{280} ratio was 0.86 ± 0.09 before purification, indicating a strong
42 presence of proteins in the loading solution. Following the purification step, the ratio improved to
43 1.85 ± 0.06 , highlighting that the eluate predominantly contained DNA hybrids free of proteins.

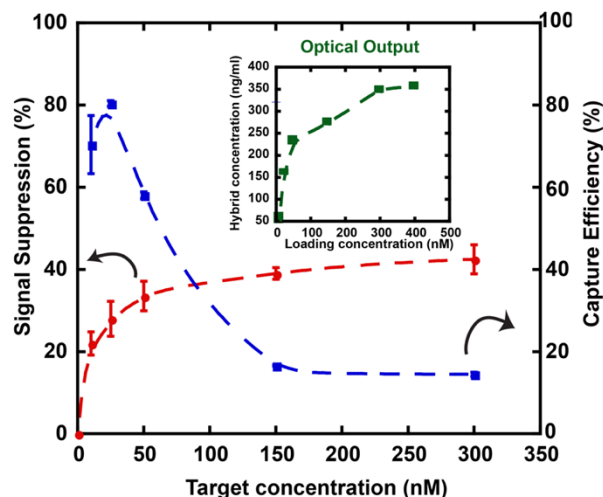


Figure 3. Electrochemical signal suppression as a function of target loading concentration; Target capture efficiency = (Hybrid concentration in eluate / target loading concentration) x 100. Inset: Hybrid concentration in eluate determined by fluorescence characterization of the duplexes with respect to the target loading concentration.

Performance in the presence of interfering DNA. A major challenge in detecting specific target sequences in a cell lysate is the presence of DNA fragments of different lengths, sequences, and concentrations. In order to mimic this scenario, we created a sample mixture model that consists of digested DNA fragments from *Lactobacillus plantarum* (a commensal bacterium common to plants, foods, and intestinal environments), FBS (10%), and the aforementioned specific TMV-derived DNA target. The genomic DNA from *Lactobacillus plantarum* was partially digested by a DNase for 30 seconds, at which digestion was stopped by heat inactivation of the enzyme. We challenged the np-Au sensing-purification platform with this complex sample to assess its detection and purification performance. As for detection, a signal suppression of ~40% was observed upon hybridization, indicating resilience to the presence of additional fragments and cellular fragments. To assess whether the purification process removed non-specific DNA fragments of various sizes in the eluate, we performed capillary electrophoresis on the sample model (before subjecting it to purification) and on the eluted hybrids (assay details in methods section). The total DNA amount for each case was kept the same by adjusting the concentration of the supplemented DNA fragments to 2.4 ng/ μ L, which is at the higher end of the concentrations

1
2
3 that the sensor can detect. The electropherograms (represented in traditional gel format) reveal
4 multiple bands corresponding to various input DNA fragments before the sample purification
5 (lanes A and C in Figure 4). In addition, lane C indicates significant signal (darker bands) possibly
6 from FBS constituents. The subsequent purification step, effectively eliminates these bands and
7 distinctive bands around the size of the 26-mer target DNA appear in lanes B and D (Figure 4).
8 The fluorescent dye binds strongly to dsDNA; therefore single-stranded target 26-mer DNA is not
9 visualized before purification. On the contrary, after purification, distinct bands corresponding to
10 26-mer hybrids appear. This is a strong indication that these are in fact 26-mer dsDNA and that
11 the np-Au device was successful in capturing the specific sequence of interest in the presence of
12 competing non-specific genomic DNA of varying sizes. It should be noted that at high ionic
13 strengths, DNA hybridization efficiency is higher due to the cation-based electrical screening of
14 the negatively-charged DNA backbone, thereby reducing repulsion between probe and target
15 strands. This may lead to decreased selectivity in target capture of the exact complementary
16 sequence. It is plausible that the selectivity can be enhanced by identifying ionic strengths that
17 minimize the hybridization of targets with slight mismatches. In addition, the drastic difference
18 between the number and intensity of bands in columns A and B in contrast to those in C and D
19 suggests that the purification step is successful in not only removing FBS components and other
20 DNA fragments, but also releasing the duplexes of the specific target DNA. For a semi-quantitative
21 comparison of the size distribution for pre- and post-purification samples, we extracted full-width
22 at half-maximum (FWHM) and full-width at fourth-maximum (FWFM) via intensity analysis of
23 the gels (Figure S4). The FWHM and FWFM centered around the target peak (26 bps) reduced
24 from 150 bps and 400 bps respectively to 13 bps and 26 bps respectively after purification,
25 highlighting successful extraction of the target duplex size.
26
27
28
29
30
31
32
33
34
35
36
37
38
39
40
41
42
43
44
45
46
47
48
49
50
51
52
53
54
55
56
57
58
59
60

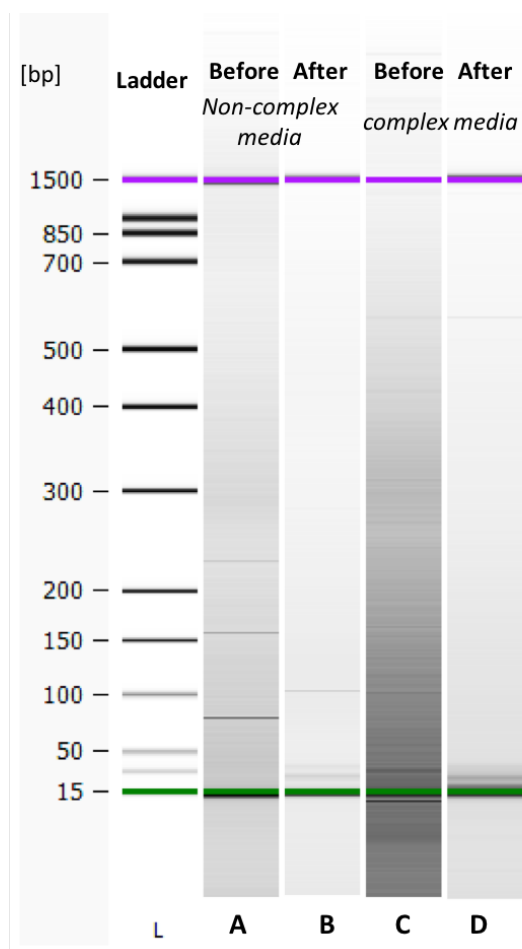


Figure 4. (A) Digested DNA fragments obtained from *Lactobacillus plantarum* were added to FBS/phosphate buffer and spiked with the 26-mer DNA target. Lane L shows the ladder with different sizes of DNA used for calibration. The upper and lower markers of the ladder are located at 15 bp and 1500 bp indicated by the green and violet bands on the gel respectively. Non-complex media: Gel lanes A and B correspond to the case where np-Au detection and purification device was used in the absence of FBS. The sample before purification containing the added genomic DNA fragments and the desired 26-mer target DNA can be seen in the lane A. After the purification, non-specific DNA fragments in the eluent are removed and the band corresponding to specific 26-mer DNA hybrids becomes dominant in lane B. The lanes C and D correspond to bands before and after purification in the presence of FBS. The lane D demonstrates that the non-specific fragment DNA and FBS components are largely eliminated and only the size around the 26-mer target DNA remains.

CONCLUSION

In summary, we demonstrated a novel platform that leverages the unique features of np-Au electrodes (i.e., biofouling resilience, lower limit of detection) to achieve integrated detection and purification of target DNA for further downstream bioanalytical analyses, such as generating specific primers for polymerase chain reaction-based sensing schemes and for isolating small DNA/RNA sequences from mixed nucleic acid populations. The electrochemical desorption technique should allow for selective elution of different probe-target pairs or the backfill molecules by modifying the linker chemistry (e.g., using selenol groups instead of thiol groups for certain types of molecules on the surface). Molecules with selenol groups can be cleaved in a different potential window thus enabling selective cleaving³⁵. Selective purification of molecules based on molecular size can also be achieved by well-established techniques to tune the np-Au morphology^{36,37}. This novel purification platform combined with the microfabrication compatibility of np-Au should enable the development of multiplexed complete sample-to-answer systems for point of care diagnostics.

EXPERIMENTAL METHODS

Chemicals and reagents

Film deposition was performed on 0.15 mm-thick glass coverslips (22 mm × 22 mm) which were purchased from Electron Microscopy Sciences. Gold, silver and chrome targets (99.95% pure) were obtained from Kurt J. Lesker. Nitric acid (70%, used as received) was obtained from Sigma-Aldrich. Sulfuric acid (96%) and hydrogen peroxide (30%) were purchased from and J. T. Baker. Piranha solution, consisting of 4:1 ratio (by volume) of sulfuric acid and hydrogen peroxide, was used for cleaning glass coverslips. CAUTION: *Piranha solution and nitric acid are highly corrosive and reactive with organic materials and must be handled with extreme care.* Tris (2-chloroethyl) phosphate (TCEP), magnesium chloride, sodium phosphate monobasic, sodium phosphate dibasic were obtained from Fisher Scientific. Methylene Blue (MB) was purchased from Sigma-Aldrich. 1X phosphate-buffered saline (PBS), composed of 137 mM NaCl, 2.7 mM KCl, 10 mM Na₂HPO₄, and 1.8 KH₂PO₄ with a pH of 7.4, was obtained from Corning. Heat-inactivated fetal bovine serum (FBS) was obtained from Life Technologies. The oligonucleotides, obtained from Integrated DNA Technologies (IDT), were 26 bases-long and the 5' end of probe ssDNA was modified with a C6 linker and thiol group. The sequences used in this study were:

1
2
3
4
5 Probe ssDNA: 5ThioMC6-D/CGT GTT ATA AAA TGT AAT TTG GAA TT;
6

7 Target DNA: AAT TCC AAA TTA CAT TTT ATA ACA CG
8
9

10 **Fabrication of nanoporous gold electrodes**

11 Nanoporous gold (np-Au) gold films were prepared by sputter deposition and subsequent
12 dealloying. Briefly, glass cover slips were cleaned in piranha solution, rinsed in deionized (DI)
13 water, and dried under nitrogen flow prior to metal deposition. Metal deposition was carried out
14 using a magneto-sputtering system (Kurt J. Lesker). First, a 160 nm-thick chrome layer was
15 sputtered at 300 W to promote adhesion between glass and the subsequent metallic layers. Next,
16 80 nm-thick seed layer of gold was sputtered at 400 W and finally silver and gold were co-sputtered
17 at 100 W and 200 W respectively to obtain a 600 nm-thick alloy layer. All depositions were
18 performed successively under argon ambient at 10 mTorr. The composition of the alloy was 64%
19 Ag and 36% Au (at. %) as determined by X-ray energy dispersive spectroscopy (EDS), (Oxford
20 Instruments). The samples were then dealloyed in 70% nitric acid at 55°C for 15 minutes to
21 produce the np-Au films and then rinsed with DI water. The substrates were then dealloyed in
22 heated nitric acid, where as silver atoms are removed, gold atoms undergo surface diffusion to
23 self-assemble into the characteristic bi-continuous open-pore gold structure³⁸. Planar gold (pl-Au)
24 electrodes were also fabricated by sputter-depositing a 50 nm-thick chrome adhesion layer
25 followed by 250 nm-thick gold film onto piranha-cleaned glass cover slips. Top and cross-
26 sectional images of np-Au electrode were captured via scanning electron microscope (FEI Nova
27 NanoSEM430) at 100 kX magnification.
28
29
30
31
32
33
34
35
36
37
38
39
40
41
42
43

44 **Sensor preparation**

45 The np-Au and planar gold electrodes were cleaned in dilute piranha solution for 20 s prior to
46 functionalization. The electrodes were then incubated in 25 mM phosphate buffer (PB), containing
47 2 μ M thiolated probe DNA and 50 mM $MgCl_2$ for 15 hours at room temperature. 1 mM
48 mercaptohexanol (MCH) prepared in PB was used as back-fill agent to passivate the surface that
49 is not covered by probe DNA. The electrodes were thoroughly rinsed with PB to remove non-
50 specifically bound DNA. DNA-functionalized electrodes were incubated in 150 μ L of 20 μ M
51 methylene blue (MB) prepared in 1X phosphate buffered saline (PBS) for control measurements
52
53
54
55
56
57
58
59
60

1
2
3 and in 1X PBS containing or 10% fetal bovine serum (FBS) for complex media experiments for
4 10 minutes. Unbound MB molecules were removed by washing with PB. The electrode was placed
5 inside a custom-built Teflon electrochemical cell and 1X PBS or 1X PBS containing 10% FBS
6 was used as the electrolyte for measurements. Probe-modified electrode was interrogated with
7 different concentrations of target DNA. The electrode was incubated with desired target DNA
8 prepared in PB containing 50 mM MgCl₂ or with the addition 10% FBS (complex media
9 experiments) for 35 minutes at 37 °C. Non-specifically-bound target molecules were removed by
10 PB rinse. The electrodes were then incubated with MB and measurements were carried out in a
11 similar fashion as the probe DNA.
12
13
14
15
16
17
18
19
20

21 **Electrochemical methods**

22 The homemade Teflon cell was utilized to carry out electrochemical measurements with a Gamry
23 Reference 600 potentiostat. Np-Au and planar Au electrodes with footprints of 0.15 cm² were
24 employed as working electrodes while platinum wire and Ag/AgCl electrodes were used as counter
25 and reference electrodes respectively. Probe grafting and target hybridization were
26 electrochemically quantified using the MB-DNA reduction peak obtained via square wave
27 voltammetry (SWV). All SWV measurements were performed in 1X PBS containing 10% FBS
28 over the potential range 0 to -0.5 V with an amplitude of 40 mV, step size of 4 mV and frequency,
29 18 Hz for np-Au and 60 Hz for planar Au. The electrodes were rinsed with PB prior to cleaving.
30 Electrochemical cleaving was done using cyclic voltammetry (CV) with 25 mM phosphate buffer
31 as the electrolyte. The potential scan range for CV was between 0 to -1.5 V.
32
33
34
35
36
37
38
39
40
41

42 **Optical quantification of hybrids: PicoGreen assay**

43 The density of the eluted hybrids was estimated using a fluorescent double-stranded DNA
44 (dsDNA) binding dye, PicoGreen. Quant-IT PicoGreen dsDNA assay kit was purchased from
45 Thermo Fisher Scientific. PicoGreen dye stock was diluted 200 fold in 1X TE buffer and used as
46 working solution. Standard curves with λDNA provided were obtained in FBS as shown in Figure
47 S2. 150 μl of eluted hybrids were collected in a microcentrifuge tube. The tube was vortexed
48 lightly and spun down to ensure uniform mixing. 20 μL of PicoGreen dye was added to 20 μl
49 aliquots of the eluted hybrids. At least 2 different aliquots were analyzed from a single cleaving
50 run. The dye and sample were mixed thoroughly and allowed to equilibrate at room temperature
51
52
53
54
55
56
57
58
59
60

1
2
3 in dark for 5 minutes. NanoDrop fluorospectrometer was used for the measurements. PicoGreen
4 exhibits an emission maximum at 530 nm upon binding to dsDNA. 2 μ l sample volume was used
5 for fluorescence quantification. The RFU values were converted to concentration values using the
6 calibration curve in Figure S2.
7
8
9

10 11 12 **Capillary electrophoresis**

13
14 In order to evaluate the efficacy of eluted hybrids in presence of other interfering DNA strands
15 and proteins, capillary electrophoresis was performed before and after purification using Agilent
16 Bioanalyzer 2100. The resulting data is translated into gel-like images (bands) which have been
17 used in this study to evaluate the presence/absence of DNA. The samples before purification
18 contain the target 26 mer DNA along with the other genomic DNA. The eluted samples (*after*) and
19 the input samples (*before*) were pre-concentrated by centrifugation and evaporation. The obtained
20 concentrations were measured using Thermo Fisher Scientific Qubit and the concentrations were
21 adjusted such that before and after samples have same similar amounts of DNA. The samples (2
22 μ l) were then loaded onto the bioanalyzer chip.
23
24
25
26
27
28
29
30
31

32 **Associated Content**

33 **Supporting Information**

34
35 Text and figures additional electrochemical results, PicoGreen optical assay calibration and
36 electrophoresis results. This material is available free of charge via the Internet at
37 <http://pubs.acs.org>
38
39
40
41

42 **Author Information**

43 **Corresponding Author**

44 *E-mail: eseker@ucdavis.edu
45
46
47

48 **Notes**

49 The authors declare no competing financial interest.
50
51
52
53
54
55
56
57
58
59
60

Acknowledgements

We gratefully acknowledge the support from UC Lab Fees Research Program Award (12-LR-237197), UC Davis Research Investments in the Sciences & Engineering (RISE) Award, and National Science Foundation Awards (CBET-1512745 and CBET&DMR-1454426). We thank Tatiana Dorofeeva for assistance in SEM imaging. We also thank Prof. Josh Hihath, Dr. Paul Feldstein, and Yuanhui Li for discussions on gold-thiol cleaving mechanisms.

References

- (1) Cederquist, K. B.; Kelley, S. O. *Current opinion in chemical biology* **2012**, *16*, 415.
- (2) Lei, J.; Ju, H. *Chemical Society Reviews* **2012**, *41*, 2122.
- (3) Zhu, C.; Yang, G.; Li, H.; Du, D.; Lin, Y. *Analytical chemistry* **2014**, *87*, 230.
- (4) Xue, Y.; Markmann, J.; Duan, H.; Weissmüller, J.; Huber, P. *Nature communications* **2014**, *5*, 1.
- (5) Tang, S.; Zhang, H.; Lee, H. K. *Analytical Chemistry* **2015**, *88*, 228.
- (6) Labib, M.; Martić, S.; Shipman, P. O.; Kraatz, H.-B. *Talanta* **2011**, *85*, 770.
- (7) Sim, J. H. C.; Anikst, V.; Lohith, A.; Pourmand, N.; Banaei, N. *Journal of clinical microbiology* **2015**, *53*, 2329.
- (8) Price, C. W.; Leslie, D. C.; Landers, J. P. *Lab on a Chip* **2009**, *9*, 2484.
- (9) J. Sambrook, D. R. *Cold Spring Harbor Laboratory Press*.
- (10) Tian, H.; Hühmer, A. F. R.; Landers, J. P. *Analytical biochemistry* **2000**, *283*, 175.
- (11) Breadmore, M. C.; Wolfe, K. A.; Arcibal, I. G.; Leung, W. K.; Dickson, D.; Giordano, B. C.; Power, M. E.; Ferrance, J. P.; Feldman, S. H.; Norris, P. M. *Analytical chemistry* **2003**, *75*, 1880.
- (12) Tanaka, N.; Kobayashi, H.; Ishizuka, N.; Minakuchi, H.; Nakanishi, K.; Hosoya, K.; Ikegami, T. *Journal of chromatography A* **2002**, *965*, 35.
- (13) Ishizuka, N.; Minakuchi, H.; Nakanishi, K.; Hirao, K.; Tanaka, N. *Colloids and Surfaces A: Physicochemical and Engineering Aspects* **2001**, *187*, 273.
- (14) Easley, C. J.; Karlinsey, J. M.; Bienvenue, J. M.; Legendre, L. A.; Roper, M. G.; Feldman, S. H.; Hughes, M. A.; Hewlett, E. L.; Merkel, T. J.; Ferrance, J. P. *Proceedings of the National Academy of Sciences* **2006**, *103*, 19272.
- (15) Cady, N. C.; Stelick, S.; Batt, C. A. *Biosensors and Bioelectronics* **2003**, *19*, 59.

- 1
2
3 (16) Reedy, C. R.; Price, C. W.; Sniegowski, J.; Ferrance, J. P.; Begley, M.; Landers, J.
4 *P. Lab on a Chip* **2011**, *11*, 1603.
5
6 (17) Witek, M. A.; Llopis, S. D.; Wheatley, A.; McCarley, R. L.; Soper, S. A. *Nucleic*
7 *acids research* **2006**, *34*, e74.
8
9 (18) Liu, D.; Liang, G.; Zhang, Q.; Chen, B. *Analytical chemistry* **2013**, *85*, 4698.
10
11 (19) Clark, K. D.; Nacham, O.; Yu, H.; Li, T.; Yamsek, M. M.; Ronning, D. R.;
12 Anderson, J. L. *Analytical chemistry* **2015**, *87*, 1552.
13
14 (20) Alla, A. J.; d'Andrea, F. B.; Bhattarai, J. K.; Cooper, J. A.; Tan, Y. H.; Demchenko,
15 A. V.; Stine, K. J. *Journal of Chromatography A* **2015**, *1423*, 19.
16
17 (21) Santos, G. M.; Zhao, F.; Zeng, J.; Li, M.; Shih, W. C. *Journal of biophotonics* **2015**,
18 *8*, 855.
19
20 (22) Yin, H.; Zhou, C.; Xu, C.; Liu, P.; Xu, X.; Ding, Y. *The Journal of Physical*
21 *Chemistry C* **2008**, *112*, 9673.
22
23 (23) Daggumati, P.; Matharu, Z.; Wang, L.; Seker, E. *Analytical chemistry* **2015**, *87*,
24 8618.
25
26 (24) Daggumati, P.; Matharu, Z.; Seker, E. *Analytical chemistry* **2015**, *87*, 8149.
27
28 (25) Seker, E.; Reed, M. L.; Begley, M. R. *Materials* **2009**, *2*, 2188.
29
30 (26) Patel, J.; Radhakrishnan, L.; Zhao, B.; Uppalapati, B.; Daniels, R. C.; Ward, K. R.;
31 Collinson, M. M. *Analytical chemistry* **2013**, *85*, 11610.
32
33 (27) Arinaga, K.; Rant, U.; Knežević, J.; Pringsheim, E.; Tornow, M.; Fujita, S.;
34 Abstreiter, G.; Yokoyama, N. *Biosensors and Bioelectronics* **2007**, *23*, 326.
35
36 (28) Singer, V. L.; Jones, L. J.; Yue, S. T.; Haugland, R. P. *Analytical biochemistry*
37 **1997**, *249*, 228.
38
39 (29) Kerman, K.; Ozkan, D.; Kara, P.; Meric, B.; Gooding, J. J.; Ozsoz, M. *Analytica*
40 *Chimica Acta* **2002**, *462*, 39.
41
42 (30) Wang, J.; Rivas, G.; Jiang, M.; Zhang, X. *Langmuir* **1999**, *15*, 6541.
43
44 (31) Moore, E. J.; Curtin, M.; Ionita, J.; Maguire, A. R.; Ceccone, G.; Galvin, P.
45 *Analytical chemistry* **2007**, *79*, 2050.
46
47 (32) Kurtulus, O.; Daggumati, P.; Seker, E. *Nanoscale* **2014**, *6*, 7062.
48
49 (33) Gittard, S. D.; Pierson, B. E.; Ha, C. M.; Wu, C. A. M.; Narayan, R. J.; Robinson,
50 D. B. *Biotechnology journal* **2010**, *5*, 192.
51
52
53
54
55
56
57
58
59
60

(34) Yeates, C.; Gillings, M.; Davison, A.; Altavilla, N.; Veal, D. *Biological procedures online* **1998**, *1*, 40.

(35) Sato, Y.; Mizutani, F. *Physical Chemistry Chemical Physics* **2004**, *6*, 1328.

(36) Tan, Y. H.; Davis, J. A.; Fujikawa, K.; Ganesh, N. V.; Demchenko, A. V.; Stine, K. J. *Journal of materials chemistry* **2012**, *22*, 6733.

(37) Dorofeeva, T.; Matharu, Z.; Daggumati, P.; Seker, E. *The Journal of Physical Chemistry C* **2016**, *120*, 4080.

(38) Erlebacher, J.; Aziz, M. J.; Karma, A.; Dimitrov, N.; Sieradzki, K. *Nature* **2001**, *410*, 450.

Table of contents graphic

